Applied Catalysis A: General 513 (2016) 9–18

Contents lists available at ScienceDirect

Applied Catalysis A: General

journal homepage: www.elsevier.com/locate/apcata

Glycerol carbonylation with CO_2 to glycerol carbonate over CeO_2 catalyst and the influence of CeO_2 preparation methods and reaction parameters

Jiaxiong Liu, Yuming Li, Juan Zhang, Dehua He*

Innovative Catalysis Program, Key Lab of Organic Optoelectronics & Molecular Engineering of Ministry of Education, Department of Chemistry, Tsinghua University, Beijing 100084, China

ARTICLE INFO

Article history:
Received 24 July 2015
Received in revised form
17 December 2015
Accepted 22 December 2015
Available online 29 December 2015

Keywords:
Glycerol
Glycerol carbonate
Carbon dioxide
CeO_2
2-cyanopyridine

ABSTRACT

The synthesis of glycerol carbonylation with CO_2 to glycerol carbonate over CeO_2 catalyst was investigated. CeO_2 with different morphologies was prepared by traditional precipitation (TP), hydrothermal (TH) and citrate sol-gel (SG) methods, and the reaction of glycerol with CO_2 was carried out in the presence of a dehydrating agent and solvent. The effect of preparation methods of CeO_2 and reaction parameters on the activity and selectivity of the catalysts were examined. The structures, morphologies and surface properties of the catalysts were characterized by XRD, TEM, BET, CO_2-TPD, H_2-TPR, Raman and XPS. CeO_2 exhibited high catalytic activity for the formation of glycerol carbonate under mild reaction conditions. The carbonylation of glycerol was influenced by the redox property of CeO_2. The effects of different types of dehydrating agent and solvent were also studied. The dehydrating agent (2-cyanopyridine) and solvent (Dimethyl Formamide(DMF)) contributed to the increase of glycerol conversion and the yield of glycerol carbonate. The yield of glycerol carbonate could reach as high as 78.9%, and the catalysts could be easily regenerated by calcination at 400 °C for 5 h without loss of activity after 5 recycling times. The proper reaction conditions were 150 °C, 4 MPa and 5 h.

1. Introduction

Glycerol, as a by-product of biodiesel manufacture, is available in a great quantity and urgently needs to be transformed to high value-added derivatives [1]. The studies for the new utilizations of glycerol are in progress, and one of which is the synthesis of glycerol carbonate. On account of its physical properties (high boiling point, water solubility, low volatility, low toxicity and biodegradability) and its reactivity as an organic chemical compound [2], glycerol carbonate has a variety of applications such as solvent, chemical intermediates, carrier in batteries and monomer for polymers [3–6].

There are several routes for the synthesis of glycerol carbonate [6], which can be divided into two categories, indirect and direct routes, according to different carbonyl sources. For the direct route (glycerol carbonylation with CO_2), it has drawn much interest because the atom utilization of this process could be as high as 87% [7] and greenhouse gas CO_2, which is an inexpensive, nontoxic and nonflammable carbon source, could be utilized [8]. The first attempt was carried out by Vieville et al. [9] using glycerol and supercritical CO_2 as reactants in the presence of zeolites and basic ion-exchange resins, but only when adding ethylene carbonate as co-reactant, could glycerol carbonate be formed. Even though the yield of glycerol carbonate could reach 32%, there was no evidence about the direct insertion of CO_2. Tin complexes [10] and metal-impregnated zeolite [11] were also reported for the carbonylation of glycerol with CO_2, but the conversion of glycerol came to only 2.5% (453 K, 5 MPa, 6 h) and 5.8% (453 K, 10 MPa, 3 h), respectively. Thermodynamic calculations showed that the low conversion of glycerol was because of the severe equilibrium limitation [12], so dehydrant or couplant should be used to break the thermodynamic limit. 13X zeolite and acetonitrile were employed for this purpose in the presence of Bu_2SnO [7], Cu/La_2O_3 [13] or Zn/Al/La/M (M = Li, Mg, Zr) hydrotalcite-like catalysts [14] and achieved enhanced results. Despite of all these progress, the conversion of glycerol is still relatively low and it is a challenge to develop new effective catalytic system.

CeO_2 is a technologically important metal oxide in virtue of its unique redox and acid-base properties [15] and often used as supports or catalysts. As the heterogeneous catalysts, CeO_2 showed

* Corresponding author. Fax: +86-010-62773346.
E-mail address: hedeh@mail.tsinghua.edu.cn (D. He).

http://dx.doi.org/10.1016/j.apcata.2015.12.030
0926-860X/

excellent performance in some catalytic reactions, such as alkylation of aromatic compounds [16], reduction of carboxylic acid [17] and dehydration of alcohols [18]. Recently, Honda et al. employed CeO_2 as the catalyst for the synthesis of various cyclic carbonates from CO_2 and diols with 2-cyanopyridine as dehydrating agent [19]. This carboxylation/hydration cascade catalytic system was also proved to be effective for the synthesis of organic carbonate from alcohols and CO_2 in the presence of 2-cyanopyridine, which worked as a remarkable dehydration reagent [20].

However, up to now, no studies have been reported concerning the synthesis of glycerol carbonate from glycerol and CO_2 over CeO_2 catalyst. In present research, we employed CeO_2 as the catalyst for the synthesis of glycerol carbonate from glycerol and CO_2 in the presence of 2-cyanopyridine, which was used as a dehydration reagent to remove water and shift the chemical equilibrium to the glycerol carbonate side. The objective of the work was to develop a new effective catalytic system to increase the reaction rate and selectivity of the carbonylation of glycerol. CeO_2 is expected to accelerate the carbonylation rate. The effects of the preparation methods of CeO_2 and the reaction parameters on the catalytic performance were investigated.

2. Experimental

2.1. General

Cerium nitrate ($Ce(NO_3)_3{\cdot}6H_2O$), citric acid, sodium hydroxide, acetonitrile (99.0%) DMF (99.5%), DMSO (99.0%), pyridine (99.0%), tetrahydrofuran (99.0%), acetone (99.5%), *n*-butyl alcohol (99.5%), ethanol (99.7%) and 25(wt)% ammonia solution were all analytical grade and purchased from Sinopharm Chemical Reagent Beijing Company. 2-cyanopyridine (99.0%), 2-picoliamide (98.0%), phenylacetonitrile (99.0%), benzonitrile (99.0%) and valeronitrile (97.5%) were bought from J&K Scientific. Glycerol (HPLC) was supplied by Alfa Aesar Company. Glycerol carbonate was obtained from TCI Chemicals. CO_2 and N_2 with a high purity of 99.999% were purchased from Beijing htjkgas Chemical Company.

2.2. Catalyst preparation

CeO_2 catalysts were prepared by precipitation, hydrothermal and citrate sol-gel method, respectively.

Precipitation method: 150 mL of 0.33 mol/L Cerium nitrate solution and an appropriate amount of 1 mol/L ammonia solution were simultaneously added into a 500 mL beaker dropwise under vigorous stirring, keeping the pH value (10 ± 1) and temperature of the suspension at 60 °C. The precursor was aged at the same temperature for 3 h, filtered and washed with deionized water for five times, and then dried at 60 °C in air for 24 h, followed by calcination at 400 °C for 5 h in air. The obtained product was denoted as CeO_2-PT-400. The samples calcined at different temperatures were named as CeO_2-PT-X(X means the calcination temperature).

Hydrothermal method: 40 mL of 6 mol/L sodium hydroxide solutions were added into 20 mL of 0.3 mol/L cerium nitrate solution in a Teflon bottle, and the mixture was kept stirring for 20 min. Subsequently, the Teflon bottle was held in a stainless steel autoclave, and then it was sealed tightly and subjected to hydrothermal treatment at 120 °C for 24 h. The obtained precipitate was centrifugally washed with deionized water, dried at 60 °C in air for 24 h, followed by calcination at 400 °C for 5 h in air to obtain CeO_2-HT-400.

Citrate sol-gel method: 50 mL of 0.5 mol/L cerium nitrate solution and 50 mL of 0.5 mol/L citric acid ethanol-water solution were added into a 250 mL beaker. The obtained solution was evaporated at 90 °C under vigorous stirring until a diaphanous sol appeared. Afterwards, the sol was dried at 60 °C for 24 h and calcined at 400 °C for 5 h in air. The sample was labeled as CeO_2-SG-400.The catalysts were regenerated by calcination in air at 400 °C for 5 h.

2.3. Catalyst characterization

The BET surface areas and pore volumes of CeO_2 samples were measured by low temperature nitrogen adsorption/desorption, using a Micromeritics TriStar II 3020 M analyzer. The measurements were performed after degassing the samples at 200 °C for 1 h under vacuum.

The powder X-ray diffraction patterns were recorded on a Rigaku D/Max-2500 diffractometer with a slit of 1° at a scanning rate of 10°/min, using Cu Kα radiation ($\lambda = 1.5406$ Å) and a nickel filter. The mean crystal size(d) was calculated by the line broadening method with the Scherrer equation $d = K\lambda/\beta\cos\theta$, where K is Scherrer constant taken as 0.89, λ is the wavelength of the X-ray, β is the width of peak at half-maximum height, and θ is the diffraction angle of CeO_2(1 1 1).

The X-ray photoelectron spectroscopies (XPS) were performed on a PHI Quantera Scanning X-ray Microprobe of ULVAC-PHI Inc., and the carbonaceous C1s line at 284.8 eV was used as the reference for the calibration of the binding energy.

The images of transmission electron microscopy (TEM) were recorded on a FEI Tecnai G^2 20 microscope operating at 200 kV. Prior to the measurement, CeO_2 samples were dispersed in ethanol ultrasonically, and then one drop of the suspension was dried in air on a copper grid. Raman spectra were measured on a HORIBA Jobin Yvon LabRAM HR Evolution instrument. The FT-IR spectra were obtained on a PerkinElmer spectrometer in the range of 400–4000 cm^{-1} using KBr as reference. The measurements of thermo gravimetric analysis (TG-DTA) were performed on TGA Q5000 V3.15 Build 263 in air with a heating rate of 10 °C/min.

The CO_2-temperature programmed desorption (CO_2-TPD) profiles were recorded by CHEMBET 3000 TPR/TPD of Quantachrome Instruments with a U-shape quartz reactor. Before the experiment, a sample was pretreated in Ar gas with a flow rate of 30 mL min^{-1} at 400 °C for 30 min. After cooling down to 100 °C, the sample was exposed to high purity of flowing CO_2 gas at 100 °C for 30 min, and then purged with flowing Ar gas at the same temperature for 30 min to remove the reversibly and physically bound CO_2. Subsequently, desorption process was carried out from 100 °C to 850 °C with a heating rate of 10 °C/min in Ar stream and the accurate flow rate was measured by soap-film flowmeter. A quadrupole mass spectrometry was used to monitor the desorbed CO_2 mass signals ($m/z = 44$), and the amount of basic sites were determined by the integrated area of CO_2-TPD peaks after calibration of the standard gases.

H_2 temperature programmed reduction (H_2-TPR) measurements were also carried out on the CHEMBET 3000 TPR/TPD instrument. Prior to the reduction, a sample was preheated in Ar gas (30 mL/min) at 400 °C for 30 min to remove surface contaminants. After cooling down to 50 °C, a mixture of 5.01%H_2/Ar was flowing through the reactor and the temperature was increased from 50 °C to 930 °C. The hydrogen consumption was monitored by a TCD detector.

2.4. catalytic reaction

All reactions were carried out in a stainless-steel autoclave with an inner volume of 100 mL. A typical procedure was as follows: 10 mmol glycerol(0.92 g), 2 mmol CeO_2(0.34 g), 30 mmol 2-cyanopyridine(3.27 g) and 10 mL DMF (Dimethyl Formamide) were added into the autoclave together, and then the reactor was sealed and placed in ice-water bath, purged with CO_2 for 3 times and then pressurized with CO_2 to 3 MPa. Afterwards, the autoclave

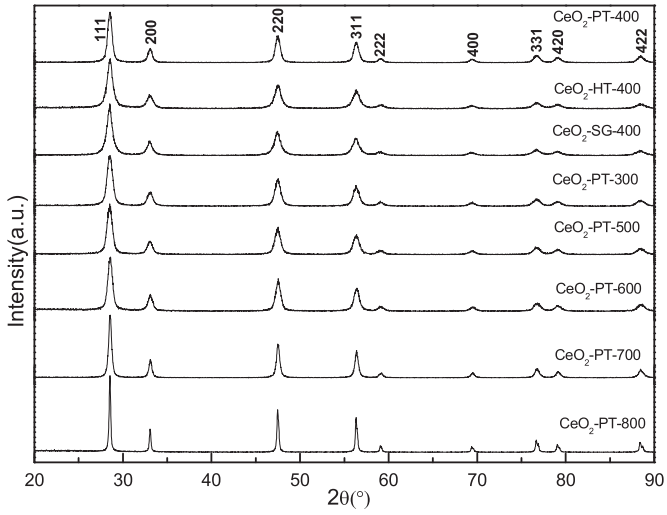

Fig. 1. XRD patterns of CeO_2 prepared by different methods and calcined at different temperature.

was heated to the reaction temperature and maintained for certain reaction time under vigorous stirring. After reaction, the reactor was cooled down to room temperature and depressurized, and certain amount of diethylene glycol monomethyl ether (DEGME) was added into the reaction mixture as an internal standard substance. After separation solid and liquid by centrifugation, the products were injected in a gas chromatography (Lunan-SP 6890) equipped with FID detector for a quantitative analysis. The column was PEG-20 M and the temperature was programmed from 90 °C to 240 °C at 10 °C min^{-1}.

The conversion of glycerol and the yield of glycerol carbonate were calculated by the following formulas:

$$X = \frac{n_{GL,in} - n_{GL,out}}{n_{GL,in}} \times 100\%$$

$$S = \frac{n_{GC,out}}{n_{GL,in}} \times 100\%$$

where X, S, $n_{GL,in}$, $n_{GL,out}$and $n_{GC,out}$ are the conversion of glycerol, yield of glycerol carbonate, mole of glycerol before reaction, mole of glycerol after reaction and mole of glycerol carbonate after reaction, respectively.

3. Result and discussion

3.1. Catalyst characterization

Crystal phases of CeO_2 catalysts prepared with different methods were investigated by XRD. Fig. 1 displays the X-ray diffractograms of the as-synthesized CeO_2 nanomaterials. All patterns can be indexed to the fluorite face-centered cubic (fcc) structure of CeO_2 (space group: Fm3m, JCPDS 34-0394). The average crystallite sizes of CeO_2 prepared by precipitation method, hydrothermal method and sol-gel method were 11.7 nm, 9.3 nm, 9.9 nm, respectively, as listed in Table 1. A detailed observation of the diffraction peaks of (1 1 1) plane (2θ at about 28.5°) revealed a slight shift toward large angle from CeO_2-SG-400 to CeO_2-PT-400 and CeO_2-HT-400.

The XRD patterns of CeO_2 synthesized with precipitation method calcined at different temperatures can be seen in Fig. 1. The crystalline structure of CeO_2 samples were not influenced by the calcination temperature and persevered with fluorite structure. But the diffraction peaks obviously narrowed down upon the increase of calcination temperature especially above 500 °C, indicating the gradual bulk sintering and growth of crystallite size of CeO_2. These

Table 1
Catalytic performance, textural properties, crystalle sizes, H_2 consumption and element conditions of CeO_2 prepared by different methods.

Catalysts	Glycerol conv.[a] (%)	Yield of glycerol carbonate[a] (%)	BET surface area ($m^2 g^{-1}$)	Pore volume[b] ($cm^3 g^{-1}$)	Average pore diameter[b] (nm)	Average crystallite size[c] (nm)	H_2 consumption[d] (umolH_2/g catalyst)	Element composition (%)[e]		Ce^{3+} concentration (%)[e]	Ce^{4+} concentration (%)[e]	Content of surface oxygen vacancies (%)[f]
								Cerium	Oxygen			
CeO_2-PT-400	30.8	29.4	59.4	0.16	9.94	11.7	72	21.0	48.9	15.1	84.9	30.21
CeO_2-HT-400	38.0	33.3	89.0	0.31	26.36	9.3	135	18.8	47.8	15.3	84.7	34.39
CeO_2-SG-400	20.7	20.5	40.6	0.09	7.61	9.9	27	19.2	48.9	13.9	86.1	29.47

[a] Reaction condition: 10 mmol glycerol, 30 mmol 2-cyanopyridine, 0.52 g catalyst, 10 mL DMF, 150 °C, 4 MPa CO_2, 5 h.
[b] Calculated using the desorption branch of the isotherm.
[c] Determined by XRD using Scherrer equation.
[d] Calculated from H_2-TPR curves(<600 °C).
[e] Calculated from the XPS patterns of Ce(3d) region.
[f] Calculated from the XPS patterns of O(1s) region.

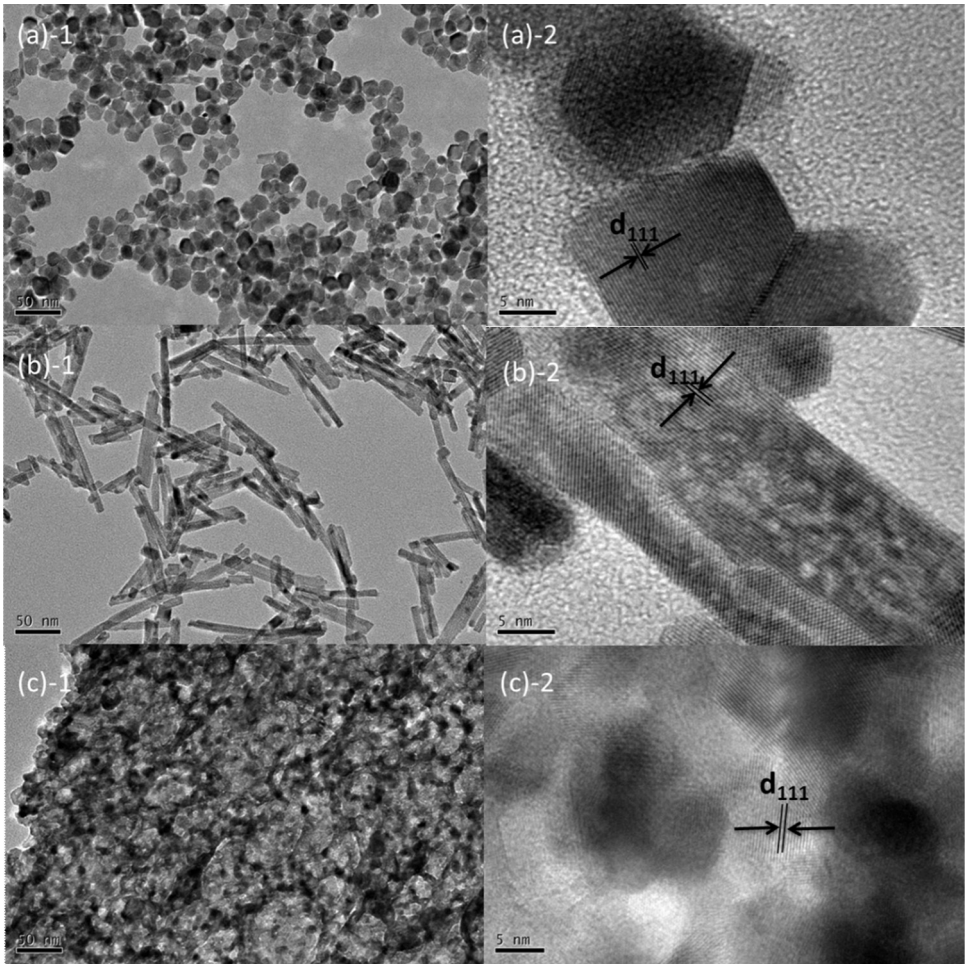

Fig. 2. TEM images of CeO_2 prepared by different methods (a) CeO_2-PT-400, (b) CeO_2-HT-400, (c) CeO_2-SG-400.

results are in accordance with the decrease of BET surface areas of CeO_2 with the increase of calcination temperature, as listed in Table S1.

The Morphology of CeO_2 prepared with various methods was examined by transmission electron microscope (TEM). The micrographs of calcined CeO_2 nanocrystals are shown in Fig. 2, from which three different morphologies can be observed: nanoparticle, nanorod and sponge-like nanomaterial, corresponding to three types of synthetic method: precipitation, hydrothermal method and sol-gel method, respectively. CeO_2 nanoparticles exhibited irregular shapes and displayed a relatively narrow size distribution of (14.6 ± 5.2) nm (Fig. 2a), and the nanorods possessed a uniform width of (8.0 ± 2.5) nm with a length of 30–100 nm (Fig. 2b), while the sponge-like CeO_2 was the agglomeration of many primary grains with diverse orientations. HRTEM analysis of CeO_2 nanoparticles and nanorods prepared with similar precipitation and hydrothermal method, respectively, by Zhou et al. [21] revealed that CeO_2 nanoparticles had two types of shape: the octahedral enclosed by eight {1 1 1} planes and the truncated octahedral enclosed by eight {1 1 1} and six {0 0 1} planes, and the predominantly exposed planes were the most stable {1 1 1} plane, whereas the CeO_2 nanorods predominantly exposed the well-defined and less stable {0 0 1} and {1 1 0} planes. Since the energy required to create oxygen vacancies on the plane has strong relevance with their stabilities, the difference of exposed plane might have effect on the catalytic performance of CeO_2 nanomaterials.

Nitrogen adsorption-desorption isotherms and the pore size distribution of CeO_2 prepared with different methods indicated that the hysteresis loops were typical type IV according to the IUPIC classification. The H3 type hysteresis loops indicated that the pores were aggregates of plate-like particle or assemblages of slit-shaped pores [22]. The pore size distribution was obtained based on BJH model. CeO_2 nanorods showed a larger average pore size at 27 nm and a broader pore size distribution while sponge-like CeO_2 had a relatively narrow pore diameter range from 2 to 4 nm, indicating that CeO_2 nanoparticles and nanorods were disordered mesopores [22,23] while sponge-like CeO_2 possessed higher degree of order. The catalysts showed large BET surface areas: 59.4 m^2/g, 89.0 m^2/g and 40.6 m^2/g for nanoparticles, nanorods and sponge-like CeO_2, respectively, as listed in Table 1. Compared with the other two preparation methods (-PT, -SG), CeO_2 prepared with hydrothermal method (-HT) showed larger surface area, pore volume and average pore diameter, which was in favor of the activation and diffusion of the reactants. Typically, metal oxide grains grew into nanocrystal through the dissolution and recrystallization at the crystal-solution interface under hydrothermal condition [24], which was beneficial of the homogenous morphology and crystallite size.

The basicity of CeO_2 was characterized by CO_2-TPD, and the profiles were shown in Fig. 3. The amount of weak, medium and strong basic sites were estimated from the integrated area under CO_2-TPD profiles in the temperature range of 20–200 °C, 200–450 °C and >450 °C, respectively. It is noticeable that the quantitative distribution of different strength basic sites and total amount of desorbed CO_2 were dramatically influenced by the preparation methods of CeO_2. A progressive increase from 55 μmol/g of CeO_2 nanoparticles to 113 μmol/g of sponge-like CeO_2 and 251 μmol/g of CeO_2

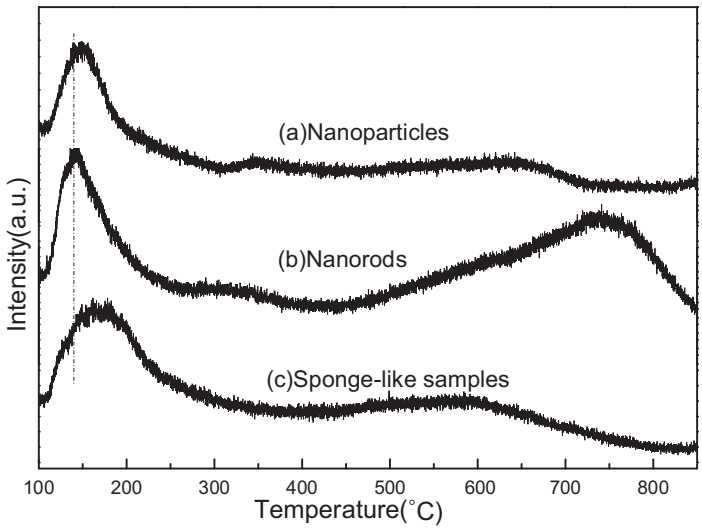

Fig. 3. CO_2-TPD profiles of CeO_2 prepared by different methods, (a) CeO_2-PT-400, (b) CeO_2-HT-400, (c) CeO_2-SG-400.

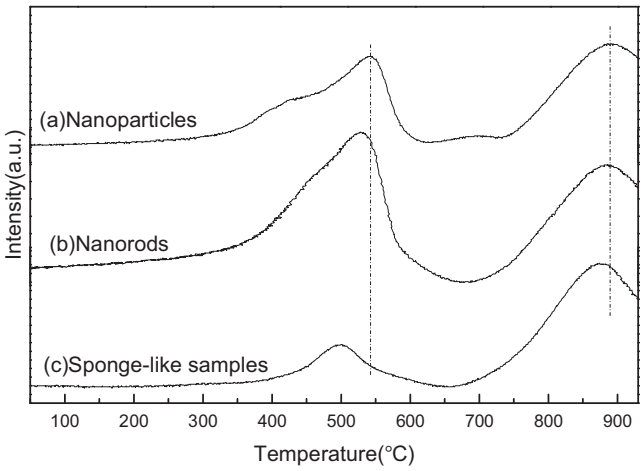

Fig. 4. H_2-TPR profiles of CeO_2 prepared by different methods (a) CeO_2-PT-400, (b) CeO_2-HT-400, (c) CeO_2-SG-400.

nanorods could be observed. In addition, the positions of weak sites displayed a slight downshift from sponge-like CeO_2 to CeO_2 nanorods. Hahn et al. [25] investigated the adsorption properties of CO_2 on a ceria (111) surface with standard DFT calculation and three stable configurations were distinguished of isolated CO_2 adsorbed on the CeO_2 surface: monodentate carbonate, bidentate carbonate and linear species. Among these three configurations, the linear species was physically adsorbed without hybridization of the CO_2 gas phase orbitals and the monodentate species was the most stable one. Since CO_2 that had stronger interaction with CeO_2 desorbed at higher temperatures [26], the low, medium and high temperature desorption peak could be assigned to linear species, bidentate carbonate and monodentate carbonate, respectively. With the basic sites of catalysts being responsible for the formation of methoxyl carbonate in the reaction of methoxyl species with CO_2 [13,27], a great deal of basicity would be favorable for the formation of glycerol carbonate.

The H_2-TPR characterization can be engaged to determine the redox ability and oxygen vacancy density of CeO_2 [23,28]. The H_2-TPR profiles of CeO_2 are depicted in Fig. 4 and the data of H_2 consumption below 600 °C is listed in Table 1. Two obvious peaks could be observed from the reduction profiles: the low-temperature peak at about 540 °C and the high-temperature peak at about 890 °C. The peak below 600 °C is generally interpreted as the surface shell reduction, including the reduction of the surface Ce from Ce^{4+} to Ce^{3+} and the formation of bridging OH groups, and the peak above 600 °C is corresponding to the bulk reduction [28]. For the CeO_2 nanoparticles, the reduction temperature of both shell and bulk shifted to slightly higher temperature compared to CeO_2 nanorods and sponge-like CeO_2, and these differences might be due to the difference of the particle size, surface area and morphology with various exposed crystal planes [28,29]. A discernable lower-temperature shoulder peak appeared at about 400 °C in the curve of CeO_2-PT-400, suggesting the heterogeneity of crystallite size distribution and smaller CeO_2 particles not detected by XRD [30]. The H_2 consumption below 600 °C could be a glancing representative of oxygen vacancy density and ranked as CeO_2-HT-400 > CeO_2-PT-400 > CeO_2-SG-400, indicating that the nanorods might have the highest oxygen storage/release capability and sponge-like CeO_2 have the lowest.

Raman spectroscopy has a very strong sensitivity to the phonon characteristics of the crystalloid which makes it a powerful tool for local structure analysis [31]. The Raman spectra of CeO_2 nanoparticles, nanorods and sponge-like CeO_2 all showed sharp peaks at 459 cm^{-1} (Fig. S1) in the spectral range from 200 cm^{-1} to 1300 cm^{-1} at an excitation wavelength of 514 nm. All three samples showed the easily identified F_{2g} mode with the highest intensity at 459 cm^{-1} as a result of symmetrical stretching mode of Ce-O vibration and three other weak band centered at 257 cm^{-1}, 594 cm^{-1} and 1173 cm^{-1} due to the second-order transverse acoustic (2TA) mode, defect sites, and second-order longitudinal optical (2LO) mode, respectively [32,33]. No obvious blue or red shift was observed between these three catalysts, but CeO_2 nanorods gave a much more asymmetric and broadened band of F_{2g} mode than nanoparticles and sponge-like CeO_2, which was induced mainly by the smaller particle size [33,34] since a linear relationship existed between the reciprocal of the effective crystallite size (d) and the full width at half maximum (FWHM) of Raman active mode peak (Γ), e.g., $\Gamma(cm^{-1}) = 10 + 124.7/d(nm)$ [35]. This result agreed with the XRD calculation data in which the crystallite size of CeO_2 nanorods was the smallest. The peak at 594 cm^{-1} was in virtue of oxygen vacancies originated from nonstoichiometry in CeO_2 [36], hence the relative intensity (I_D/I_{F2g}) could be an index of the defect sites concentration [33,35]. The ratio of I_D/I_{F2g} followed the sequence: nanorods (0.0742) > nanoparticles (0.0316) > sponge-like CeO_2 (0.0279), and the trend is same for H_2 consumption below 600 °C in TPR profile, demonstrating that

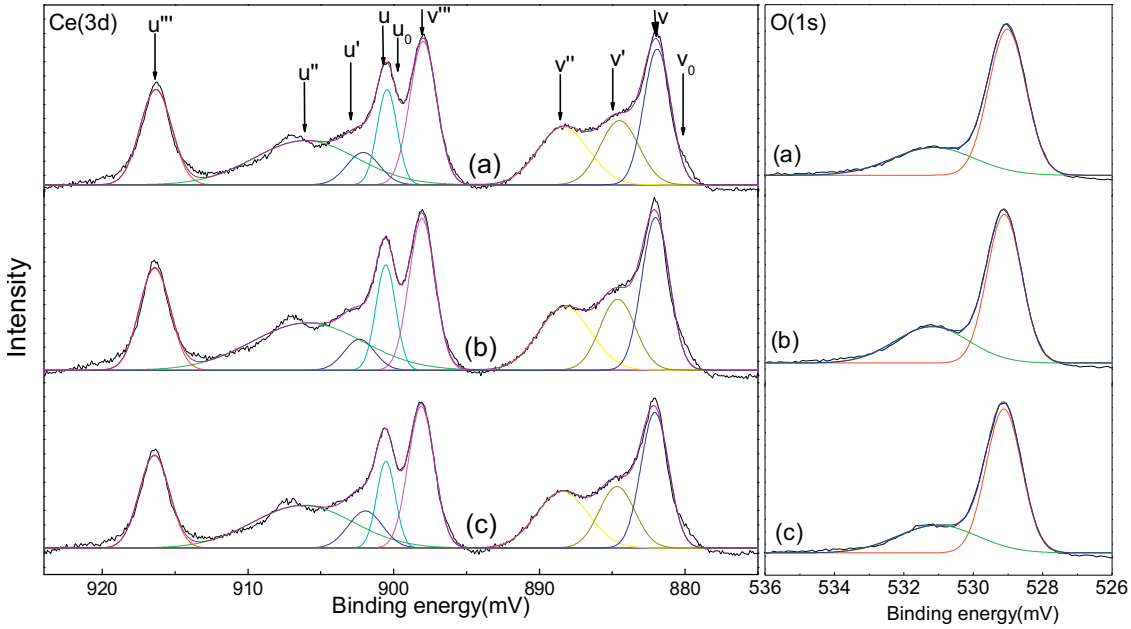

Fig. 5. XPS spectra of the Ce(3d) and O(1s) region of CeO_2 prepared by different methods (a) CeO_2-PT-400, (b) CeO_2-HT-400, (c) CeO_2-SG-400.

nanorods had the most abundant concentration of defect site while sponge-like CeO_2 had the least.

In order to reveal the chemical state of cerium on the catalyst surface, the three as-prepared CeO_2 samples were investigated by XPS. The XPS patterns of Ce(3d) and O(1s) region are illustrated in Fig. 5. For cerium, the deconvoluted peaks fitted with Gaussian function consisted of ten peaks, which can be categorized into two series: Ce^{4+} ($3d_{5/2}$) and Ce^{3+} ($3d_{3/2}$) ionic states. The corresponding peaks to each ion, their binding energies and each initial and final state [37] are presented in Table S2. The binding energy of each peak was in good consistent with the reported data [37,38] and had limited distinction between CeO_2 nanoparticles, nanorods and sponge-like samples. The ionic concentration of Ce^{3+} was semi-quantitatively analyzed via the following equation [28]:

$$[Ce^{3+}]\% = \frac{A_{v0} + A_{v'} + A_{u0} + A_{u'}}{\sum_i (A_{vi} + A_{ui})}$$

A_i, denoted as the area of the respective peaks. Element composition and the calculated concentration of Ce^{3+} and Ce^{4+}components are compiled in Table 1. CeO_2 nanoparticles and nanorods had almost the same percentage of Ce^{3+}, which was slightly higher than that in sponge-like CeO_2. The small quantities of low-coordinated Ce site in consequence of complete oxidation of the catalysts demonstrated the relatively low concentration of defect sites or oxygen vacancies, which agreed with the Raman results.

The O(1s) spectra was composed of two overlapping peaks. The main peak with lower binding energy of 529.1 eV roots in the lattice oxygen with Ce^{4+} ions [39]. The lower intense peak at 531.2 eV was assigned to different attributions: CO_3^{2-} contamination [40], hydroxyl contamination [41], highly polarized oxygen around the defect site [42] and oxygen vacancies in metal oxides [39]. The last one was more receivable in consideration of our experimental conditions. The content of the surface oxygen vacancies in the total surface oxygen was estimated from the relative integrated area, as shown in Table 1. It can be noticed that CeO_2 nanorods possessed the higher content of surface oxygen vacancies, which was in accordance with the Ce(3d) XPS analysis, Raman and H_2-TPR results.

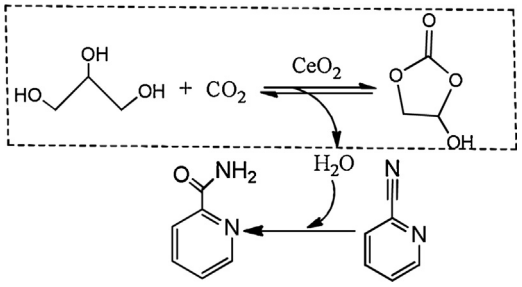

Scheme1. Carboxylation of glycerol and hydration of 2-cyanopyridine over CeO_2 catalyst.

3.2. Catalytic performance of CeO_2 prepared by different methods

Glycerol carbonate was obtained from the carbonylation of glycerol and CO_2 over CeO_2 catalysts with the hydrolysis of 2-cyanopyridine as the coupling reaction. As shown in Scheme 1, in the CeO_2/2-cyanopyridine system, glycerol reacts with CO_2 to form glycerol carbonate and H_2O, while the formed H_2O reacts with 2-cyanopyridine to be removed from the reaction system. The identification of glycerol, glycerol carbonate, 2-cyanopyridine and 2-picolinamide were determined by GC–MS and also corroborated by retention times of the standard samples via gas chromatograph. The esters which was the possible byproduct through the reaction of alcohols with 2-picolinamide [19] were barely traceable. Therefore, in all the cases, the material balance of glycerol and 2-cyanopyridine were (95 ± 5)% and (99 ± 1)%, respectively.

The catalytic performances of CeO_2 prepared with different methods in the reaction of glycerol and CO_2 in the presence of 2-cyanopyridine are listed in Table 1. High yield of glycerol carbonate was achieved over CeO_2. Additionally, CeO_2 of diverse morphology exhibited disparate activation for the formation of glycerol carbonate and ranked as CeO_2 nanorods > nanoparticles > sponge-like. The conversion of glycerol and yield of glycerol carbonate were obviously correlated with the surface area, but the relationships were not linear. The conversions of glycerol were 1.99×10^{-2}, 1.64×10^{-2} and 1.96×10^{-2} mmol/(m^2 h) and the yields of glycerol carbonate were 1.90×10^{-2}, 1.43×10^{-2} and

1.94×10^{-2} mmol/(m^2 h) for CeO_2-PT-400, CeO_2-HT-400 and CeO_2-SG-400, respectively. The data showed that the activity and selectivity of the catalysts seemed to be influenced by other factors other than the surface area. The acid-base and defect sites are generally considered to be the active center [15], hence the catalytic performance of CeO_2 was connected to its basic site amount measured from CO_2-TPD and relative oxygen vacancies characterized from H_2-TPR or Raman spectra. CeO_2 nanorods with the most abundant basic sites and oxygen vacancies gave the highest yield of glycerol carbonate, and sponge-like CeO_2 with the medium basic sites and least defect sites gave the lowest, indicating that the oxygen vacancies played a role in the catalytic system and in the meantime the acid-base property also showed effect on the activity of the catalysts. Zhang et al. [43] used Cu-based catalysts in the direct carbonylation of glycerol carbonate and demonstrated that the catalysts with Lewis base sites tended to favor the formation of glycerol carbonate. Honda et al. [19] proposed the reaction mechanism of 1,2-propanediol reacting with CO_2 over CeO_2, in which one OH group of glycerol was adsorbed onto the Lewis acid sites of CeO_2, indicating the importance of acid-base property of CeO_2 in the synthesis of propylene carbonate.

Besides the redox and acid-base properties, particle size was also to be a contributing factor for the activity of CeO_2. The crystallite size of CeO_2 nanoparticles was controlled via changing calcination temperature, and the results were presented in Fig. 6. With increasing calcination temperature from 300 °C to 500 °C, the crystallite size hardly changed, and the conversion of glycerol were almost the same, and with increasing calcination temperatures from 500 °C to 800 °C, the crystallite size grew strikingly from 11.8 nm to 48.3 nm, leading to the sharp decrease of glycerol conversion from 28.2% to 6.9%. The slight drop of activity over CeO_2 nanoparticles calcined at 200 °C is probably due to the heterogeneity of crystallite size distribution which is supported by the shoulder peak in the H_2-TPR profile [30]. Studies [44,45] had verified that decline in crystallite size would result in larger surface area and improve the amount of reactive edge sites such as oxygen vacancies which could be supported by the I_D/I_{F2g} value calculated from the Raman spectra, and could be an unexceptionable explanation for the nano-size effect in present catalytic system.

Since the carbonylation of glycerol with CO_2 is limited by thermodynamics, the coupling reactions or dehydrating agents are necessary to shift the equilibrium to desired products. Only 3.4% of glycerol carbonate yield was obtained over CeO_2 without addition of dehydrating agent, thus the outstanding yield of glycerol carbonate over CeO_2 was mainly attributed to the hydration of 2-cyanopyridine. The effect of several dehydrating agents including acetonitrile, valeronitrile, benzonitrile, phenylacetonitrile and 2-cyanopyridine was examined at reaction condition of 10 mmol glycerol, 30 mmol nitriles, 0.34 g CeO_2-PT-400, 10 mL DMF, 150 °C, 4 MPa, 5 h, and the yields of glycerol carbonate were 5.2%, 4.7%, 5.6%, 5.3% and 20.8%, respectively. Nitriles especially 2-cyanopyridine showed remarkable effect on the formation of glycerol carbonate. The high-efficiency hydration of 2-cyanopyridine above other nitriles could be ascribed to the relatively strong alkalinity and formation of intramolecular hydrogen bonding in the produced amide [20]. Effect of the amount of 2-cyanopyridine was also examined, as shown in Fig. 7. With increasing the amount of 2-cyanopyridine from 5 mmol to 30 mmol, the yield of glycerol carbonate increased dramatically from 9.5% to 19.7%. This might be due to the complete removal of water from reaction media via the hydrolysis of 2-cyanopyridine [20] resulting in elimination of thermodynamic constraint of the reaction of glycerol with CO_2. Further increasing the addition amount of 2-cyanopyridine from 30 mmol to 100 mmol gave much slower increase of conversion of glycerol, and the yield of glycerol carbonate was only increased from 19.7% to

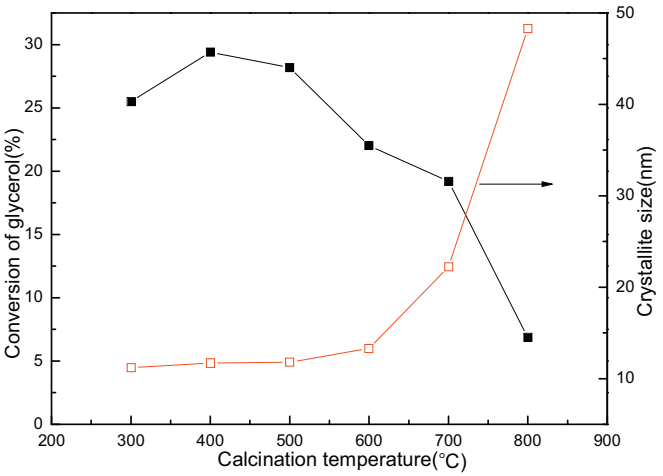

Fig. 6. Effect of calcination temperatures on crystallite size and catalytic performance of CeO_2-PT (Reaction condition: 10 mmol glycerol, 30 mmol 2-cyanopyridine, 0.52 g CeO_2, 10 mL DMF, 150 °C, 4.0 MPa CO_2, 5 h).

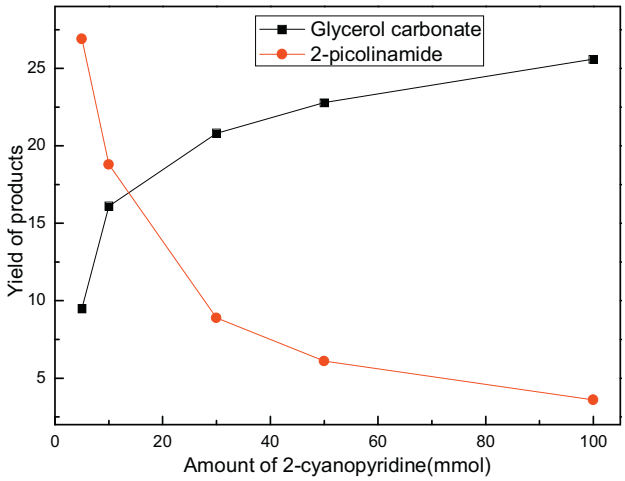

Fig. 7. Effect of the amounts of 2-cyanopyridine on the carbonylation of glycerol with CO_2 over CeO_2-PT-400 (Reaction condition: 10 mmol glycerol, 0.34 g CeO_2, 10 mL DMF, 150 °C, 4 MPa CO_2, 5 h).

25.6%, indicating that an appropriate amount of 2-cyanopyridine was obligatory for higher yield of desired product. CeO_2 prepared by different methods showed different catalytic performance in the hydration of 2-cyanopyridine (Reaction condition: 30 mmol 2-cyanopyridine(3.26 g), 30 mmol H_2O(0.54 g), 0.08 g catalysts, 10 mL DMF, 150 °C, 4 MPa CO_2, 1 h), and the yields of 2-picolinamide were 58.7%, 61.6% and 40.5% for CeO_2-PT-400, CeO_2-HT-400 and CeO_2-SG-400, respectively. The activity sequences were consistent with their catalytic performance in the carbonylation of glycerol with CO_2 in the presence of 2-cyanopyridine, demonstrating the major role of dehydration effect of 2-cyanopyridine for the formation of glycerol carbonate. CeO_2 nanorods with the most abundant oxygen vacancies gave the highest yield of 2-picolinamide, while sponge-like CeO_2 with the least defect sites gave the lowest, indicating that the redox property of CeO_2 might make a difference to their catalytic activity in the hydration of 2-cyanopyridine. The mechanism and active sites of CeO_2 for the hydration of 2-cyanopyridine were investigated by Tamura et al. [46]. and they concluded that the active sites was the Ce_{LC}-O pair site, which was the pair site of the low-coordinated Ce cation as a Lewis acid site (oxygen defect site) and adjacent oxygen as a Lewis base site. Scilicet, the hydrolysis performance of 2-cyanopyridine had strong correlation with the

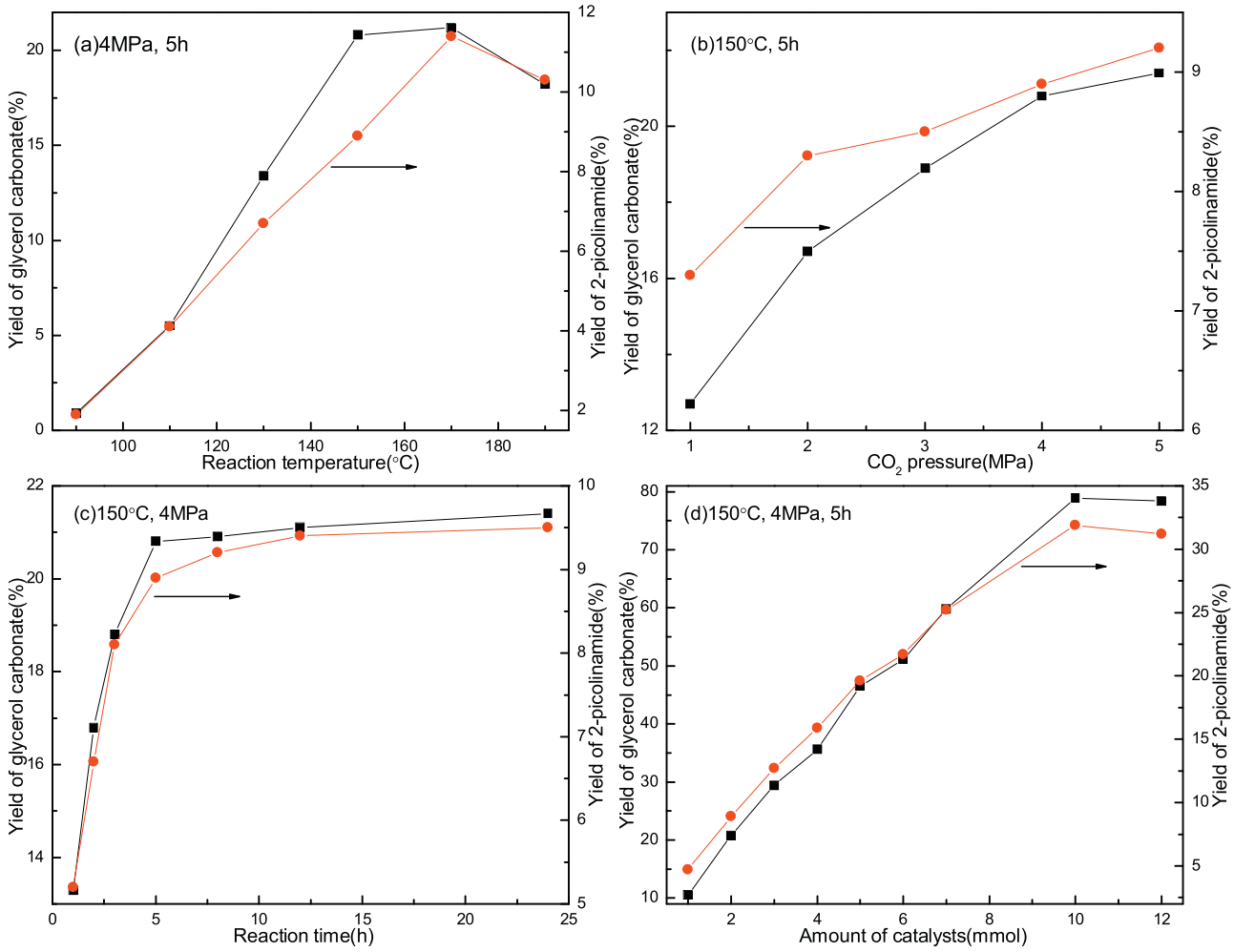

Fig. 8. Effect of (a) reaction temperature, (b) CO_2 pressure, (c) reaction time, (d) amount of catalyst on carbonylation of glycerol with CO_2 over CeO_2-PT-400 (Reaction condition: 10 mmol glycerol, 30 mmol 2-cyanopyridine, 0.34 g CeO_2 for (a), (b) and (c), 10 mL DMF).

concentration of oxygen vacancies (defect sites) and the amount of basic sites, which was in good agreement with our aforementioned results.

Furthermore, the solvent effect was also investigated. Different catalytic performance was observed when no solvent, ethanol, *n*-butyl alcohol, acetone, tetrahydrofuran, pyridine, DMSO and DMF were used as solvent and the yields of glycerol carbonate were 8.1%, 8.9%, 6.1%, 8.0%, 13.4%, 11.0%, 16.5% and 20.8% (Reaction condition: 10 mmol glycerol, 30 mmol 2-cyanopyridine, 0.34 g CeO_2-PT-400, 10 mL solvent, 150 °C, 4 MPa, 5 h), respectively. Poor conversion and mass-balance of glycerol were gained when no solvent was applied. Among the solvents employed in this study, DMF gave the maximum yield of glycerol carbonate, and DMSO gave the secondary, indicating that the solvent effect in our CeO_2/2-cyanopyridine system was one of the important factors responsible for the much better catalytic performance. Solvents usually show some effects on reaction rates, chemical equilibrium as well as reaction mechanisms in organic reactions. It had been proposed that for 1,2-propanediol reacting with CO_2 to form propylene carbonate over CeO_2 in the presence of 2-cyanopyridine [19], nucleophile attack of the other OH group to the carbonyl carbon in carbonate species, which led to the production of cyclic carbonate and water, was one of the important steps in the proposed reaction mechanism. Since the nucleophilicity of the reactants was affected in dipolar aprotic solvent [47], the step mentioned above could be enhanced in DMF and DMSO. On the other hand, the solubility of CO_2 in the solvents might also be an important factor besides the polarity and aprotic properties of the solvents. The basic nature of DMF may favor the dissolving and adsorption of CO_2. In fact, the solubility of CO_2 in DMF is 31.1 mol% at 40 °C and 4.5 MPa [48], which is larger than that in ethanol (28.1 mol% at 35 °C and 4.4 MPa) and *n*-butyl alcohol (28.7mol% at 35 °C and 4.2 MPa) [49]. Therefore, high solubility of CO_2 in DMF might be favorable to increase the concentration of CO_2 on the surface of the catalysts, consequently benefiting to the reaction.

3.3. *Influence of reaction paramers*

The effect of reaction temperatures was also investigated in the range from 90 °C to 190 °C, and the results were shown in Fig. 8(a). Glycerol carbonate yield reached the maximum at 170 °C. In the range of 90 °C to 170 °C, glycerol carbonate yield increased remarkably from 0.9% to 21.2% with the rise of reaction temperature. In contrast, the yield of glycerol carbonate decreased with higher reaction temperature above 170 °C and the material balance of glycerol deteriorated, possibly owing to the emergence of side reactions, indicating that a reasonably higher reaction temperature benefited the synthesis of glycerol carbonate.

Fig. 8(b) shows the effect of CO_2 pressures in the range from 1.0 MPa to 5.0 MPa. Glycerol carbonate yield increased from 12.7% to 20.8% with the increasing of CO_2 pressure from 1.0 MPa to

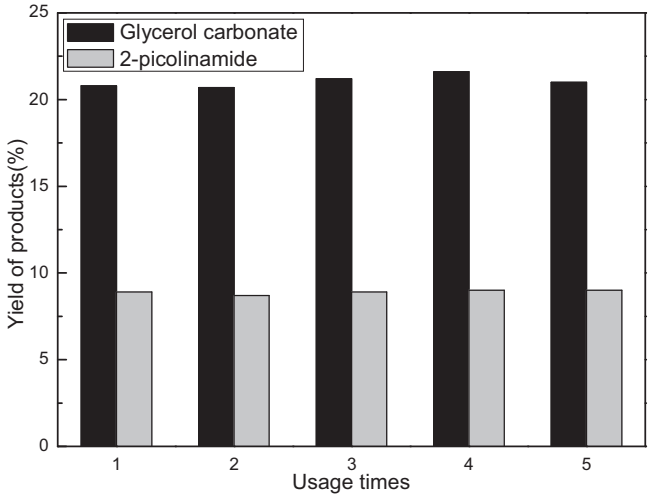

Fig. 9. Recyclability of CeO_2-PT-400 (Reaction condition: 10 mmol glycerol, 30 mmol 2-cyanopyridine, 0.34 g CeO_2, 10 mL DMF, 150 °C, 4 MPa CO_2, 5 h).

4.0 MPa, while in the range of 4.0–5.0 MPa CO_2 pressure, the increase of glycerol carbonate yield was not distinct.

The effect of reaction time under the typical conditions is illustrated in Fig. 8(c). The yield of glycerol carbonate increased from 13.3% to 20.8% as the reaction time varied from 1 h to 5 h, and then remained almost constant within 5–24 h.

The effect of catalyst amounts was examined at the conditions of 150 °C and 4.0 MPa, as shown in Fig. 8(d). With the increase of catalyst addition amounts from 0.17 g to 1.72 g, the yields of glycerol carbonate increased linearly from 10.5% to as high as 78.9%, and after that, the increasing trend became flat with more catalyst input.

In addition, the used catalysts were recovered, washed with ethanol and dried at 60 °C for 24 h, but they showed great loss of activity (yield of glycerol carbonate was 4.1% for the used CeO_2-PT-400, only 1/4 of the fresh catalyst.). Thus a deactivation of CeO_2 occurred in the CeO_2/2-cyanopyridine/DMF system. One possible reason might be that the produced amide, such as benzamide [50], was adsorbed on the CeO_2 surface and poisoned the active sites of CeO_2. But 2-picolinamide was proved to have little influence on the catalytic performance of CeO_2 in the formation of DMC from methanol and CO_2, due to the intramolecular hydrogen bonding between H atom in amide group and N atom in pyridine ring, leading to the reduction in the acidity of amides and making the adsorption weak [20]. In order to further investigate the used catalysts, XRD, BET surface area, FT-IR and TG-DTG characterizations were conducted. BET surface areas and XRD profiles (Fig. S2) were unchanged for the catalysts before and after the reaction with 2-cyanopyridine or acetonitrile as dehydrating agent, suggesting that the nanostructure of CeO_2 was stable under the reaction conditions. The IR spectra of the used catalysts showed no obvious sign of adsorption of amides with respect to that of the fresh one (Fig. S11), but the peak of hydroxyl became noticeably larger. In the TG-DTG analysis (Fig. S12), fresh CeO_2 before reaction showed weight loss of 3.29 wt%, due to the removal of adsorbed water and CO_2. CeO_2 after the reaction in the presence of 2-cyanopyridine presented a little bigger weight loss of 3.59 wt% and two obvious DTG peaks in the range of 150 °C to 350 °C. Combining with the color change (pale yellow before reaction and light brown after reaction) of the catalysts before and after reaction, one of the double peaks around 200 °C could be assigned to the adsorption of 2-cyanopyridine. The other might be the decomposition of hydroxyl or carbonate species formed by the adsorption of H_2O or CO_2 [46]. Acetonitrile adsorbed on CeO_2 provided a weight loss of 3.48% and two similar DTG peaks appeared from 150 °C to 350 °C. The attribution of these two peaks was similar to the former one. These results demonstrated that the activity loss of CeO_2 was due to the strong adsorption of nitriles on the active sites of the catalysts.

For the recycle use of CeO_2, the regeneration of spent catalysts was performed by calcination at 400 °C for 5 h. The recyclability of CeO_2 nanoparticles was verified as shown in Fig. 9. The yield of glycerol carbonate and 2-picolinamide over regenerated CeO_2 stayed practically the same as that of the fresh one even after recirculation for five times. ICP results confirmed that the leaching of CeO_2 was below the detection limit, indicating that the microstructure of the catalyst was stable and the active sites were easily regenerated by a simple calcination procedure.

4. Conclusion

CeO_2 nanoparticles, nanorods and sponge-like samples were synthesized by traditional precipitation, hydrothermal and citrate sol-gel methods, respectively. All three samples showed excellent catalytic performance in the carbonylation of glycerol and CO_2 with 2-cyanopyridine as a dehydrating agent. The incredibly high yield of glycerol carbonate had strong relevance with the efficient hydration of 2-cyanopyridine and solvent effect of DMF. Redox properties of CeO_2 played an important role on the activity of CeO_2. The proper reaction conditions were 3.26 g 2-cyanopyridine (3 times of stoichiometric value), 150 °C, 4 MPa and 5 h. The spent catalyst could be easily regenerated through the calcination process at 400 °C for 5 h, and the activity of the regenerated catalyst stayed constant even after recycling for 5 times.

Acknowledgments

We acknowledge the financial support for this work from the National Natural Science Foundation of China (No. 21573120) and the National Basic Research Program of China (973 Program, 2011CB201405) and Specialized Research Fund for the Doctoral Program of Higher Education of Ministry of Education of China (20131018984).

Appendix A. Supplementary data

Supplementary data associated with this article can be found, in the online version, at http://dx.doi.org/10.1016/j.apcata.2015.12.030.

References

[1] A. Behr, J. Eilting, K. Irawadi, J. Leschinski, F. Lindner, Green Chem. 10 (2008) 13–30.
[2] J. Ochoa-Goímez, O. Goímez-Jimeínez-Aberasturi, C. Ramírez-Loípez, M. Belsue, Org. Process Res. Dev. 16 (2012) 389–399.
[3] B. Schaffner, F. Schaffner, S.P. Verevkin, A. Borner, Chem. Rev. 110 (2010) 4554–4581.
[4] A.S. Kovvali, K.K. Sirkar, Ind. Eng. Chem. Res. 41 (2002) 2287–2295.
[5] D.P. Abraham, Electrolytes for lithium and lithium-ion batteries, U.S. Patent Appl. 2011/0117445A1 (2011).
[6] M.O. Sonnati, S. Amigoni, E. de Givenchy, T. Darmanin, O. Choulet, F. Guittard, Green Chem. 15 (2013) 283–306.
[7] J. George, Y. Patel, S.M. Pillai, P. Munshi, J. Mol. Catal. A-Chem. 304 (2009) 1–7.
[8] T. Sakakura, J.C. Choi, H. Yasuda, Chem. Rev. 107 (2007) 2365–2387.
[9] C. Vieville, J.W. Yoo, S. Pelet, Z. Mouloungui, Catal. Lett. 56 (1998) 245–247.
[10] M. Aresta, A. Dibenedetto, C. Nocito, F. Pastore, J. Mol. Catal. A-Chem. 257 (2006) 149–153.
[11] L.P. Ozorio, et al., Appl. Catal. A-Gen. (2014).
[12] J.B. Li, T. Wang, J. Chem. Thermodyn. 43 (2011) 731–736.
[13] J. Zhang, D. He, J. Colloid Interface Sci. 419 (2014) 31–38.
[14] H.G. Li, D.Z. Gao, P. Gao, F. Wang, N. Zhao, F.K. Xiao, W. Wei, Y.H. Sun, Catal. Sci. Technol. 3 (2013) 2801–2809.
[15] S. Sato, F. Sato, H. Gotoh, Y. Yamada, ACS Catal. 3 (2013) 721–734.
[16] M. Kobune, S. Sato, R. Takahashi, J. Mol. Catal. A-Chem. 279 (2008) 10–19.
[17] Y. Sakata, V. Ponec, Appl. Catal. A-Gen. 166 (1998) 173–184.

[18] H. Gotoh, Y. Yamada, S. Sato, Appl. Catal. A-Gen 377 (2010) 92–98.
[19] M. Honda, M. Tamura, K. Nakao, K. Suzuki, Y. Nakagawa, K. Tomishige, ACS catal. 4 (2014) 1893–1896.
[20] M. Honda, M. Tamura, Y. Nakagawa, K. Nakao, K. Suzuki, K. Tomishige, J. Catal. 318 (2014) 95–107.
[21] K. Zhou, X. Wang, X. Sun, Q. Peng, Y.D. Li, J. Catal. 229 (2005) 206–212.
[22] K.S.W. Sing, D.H. Everett, R.A.W. Haul, L. Moscou, R.A. Pierotti, J. Rouquerol, T. Siemieniewska, Pure Appl. Chem. 57 (1985) 603–619.
[23] A. Xie, W. Liu, S. Wang, X. Liu, J. Zhang, Y. Yang, Mater. Res. Bull. 59 (2014) 18–24.
[24] A.V. Mccormick, A.T. Bell, Catal. Rev. Sci. Eng. 31 (1989) 97–127.
[25] K.R. Hahn, M. Iannuzzi, A.P. Seitsonen, J. Hutter, J. Phys. Chem. 117 (2013) 1701–1711.
[26] V.R. Choudhary, V.H. Rane, J. Catal. 130 (1991) 411–422.
[27] D. Delledonne, F. Rivetti, U. Romano, Appl. Catal. A-Gen. 221 (2001) 241–251.
[28] N. Sutradhar, A. Sinhamahapatra, S. Pahari, M. Jayachandran, B. Subramanian, H.C. Bajaj, A.B. Panda, J. Phys. Chem. 115 (2011) 7628–7637.
[29] H. Li, G. Lu, Q. Dai, Y. Wang, Y. Guo, Y. Guo, ACS Appl. Mater. Interface 2 (2010) 838–846.
[30] F. Ying, S. Wang, C.T. Au, S.Y. Lai, Microporous Mesoporous Mater. 142 (2011) 308–315.
[31] V. Grover, R. Shukla, D. Jain, S.K. Deshpande, A. Arya, C.G.S. Pillai, A.K. Tyagi, Chem. Mater. 24 (2012) 2186–2196.
[32] W.H. Weber, K.C. Hass, J.R. Mcbride, Phys. Rev. B 48 (1993) 178–185.
[33] Z. Wu, M. Li, J. Howe, M.H. Meyer III, H.O. Steven, Langmuir 26 (2010) 16595–16606.
[34] G.W. Graham, W.H. Weber, C.R. Peters, R. Usmen, J. Catal. 130 (1991) 310–313.
[35] B. Choudhury, A. Choudhury, Mater. Chem. Phys. 131 (2012) 666–671.
[36] Z.V. Popovic, Z.D. Mitrovic, M.J. Konstantinovic, M. Scepanovic, J. Raman Spectrosc. 38 (2007) 750–755.
[37] R. Leppelt, B. Schumacher, V. Plzak, M. Kinne, R.J. Behma, J. Catal. 244 (2006) 137–152.
[38] S. Tsunekawa, T. Fukuda, A. Kasuya, Surf. Sci. 457 (2000) L437–L440.
[39] V. Grover, R. Shukla, Renu Kumari, B.P. Mandal, P.K. Kulriya, S.K. Srivastava, S. Ghosh, A.K. Tyagi, D.K. Avasthi, Phys. Chem. Chem. Phys. 16 (2014) 27065–27073.
[40] X.Y. Du, W.C. Li, Z.X. Liu, K. Xie, Chin. Phys. Lett. 5 (1999) 376–377.
[41] A. Pfau, K.D. Schierbaum, Surf. Sci. 321 (1994) 71–80.
[42] M. Skoda, M. Cabal, I. Matolinova, T. Skala, K. Veltruska, V. Matolin, Vacuum 84 (2010) 8–12.
[43] J. Zhang, D. He, J. Chem. Technol. Biotechnol. 90 (2015) 1077–1085.
[44] S.Y. Lai, Y. Qiu, S. Wang, J. Catal. 237 (2006) 303–313.
[45] S. Deshpande, S. Patil, S.V.N.T. Kuchibhatla, S. Seal, Appl. Phys. Lett. 87 (2005) 133113.
[46] M. Tamura, A. Satsuma, K. Shimizu, Catal. Sci. Technol. 3 (2013) 1386–1393.
[47] A.J. Parker, Q. Rev, Chem. Soc. 16 (1962) 163–187.
[48] A. Kordikowski, A.P. Schenk, R.M. Van Nielen, C.J. Peters, J. Supercrit. Fluids 8 (1995) 205–216.
[49] X. Gui, Z.G. Tang, W. Fei, J. Chem. Eng. Data 56 (2011) 2420–2429.
[50] M. Honda, S. Kuno, S. Sonehara, K. Fujimoto, K. Suzuki, Y. Nakagawa, K. Tomishige, ChemCatChem 3 (2011) 365–370.